Penerbit UTHM

© Universiti Tun Hussein Onn Malaysia Publisher's Office

JAMEA

http://penerbit.uthm.edu.my/ojs/index.php/jamea

e-ISSN : 2716-6201

Journal of Advanced Mechanical Engineering Applications

Numerical Analysis of Wake Interaction of Darrieus Tidal Turbine in Shallow Water Application

Najwa Syafiqa Marzuki[1], Anas Abdul Rahman[1*], Ayu Abdul-Rahman[2], Azzim Rosli[1], Syahfiq Misran[1], Wan Muhammad Fadhli Arif[1], Ramadhan Ahmed Ramadhan Basiddiq[1]

[1]Mechanical Engineering Program, Faculty of Mechanical Engineering & Technology, Universiti Malaysia Perlis, Pauh Putra Main Campus, 02600 Perlis, MALAYSIA

[2]Department of Mathematics and Statistics, School of Quantitative Sciences, Universiti Utara Malaysia, 06010 UUM, Sintok, Kedah, MALAYSIA

*Corresponding Author

DOI: https://doi.org/10.30880/jamea.2022.03.02.011
Received 27 September 2022; Accepted 29 November 2022; Available online 13 December 2022

Abstract: Malaysia is rich in natural resources including coal and fossil fuels. These natural resources, however, will diminish and pollute the ecosystem. Thus, researchers have proposed the use of renewable energy sources such as solar, wind, wave, and other energies as potential solutions to resolve the issue. This study focuses on tidal energy, specifically the vertical axis tidal turbine (VATT) for shallow water application. While a majority of the VATT research shows that this device can work effectively in deep water, its effectiveness in shallow water has yet to be explored comprehensively. To analyse the turbine's performance, Computational Fluid Dynamics (CFD) method was applied. The Darrieus turbine was used in this study since it is the ideal turbine design for shallow water in Malaysia with an average current speed of 1.0 ms^{-1}. The Darrieus turbine model used in this project is 5 metres tall and 4.3 metres in diameter. The simulation was evaluated based on wake characteristics. The Darrieus turbine was designed using the NACA0018 airfoil. Following the results of single turbine analysis, the wake has recovered to its ambience velocity at 60 metres behind the device. The wake generation due to the multi-row configuration of the devices was also examined. The three-turbine configuration verifies the concept that installing two turbines side by side boosts the performance significantly. Notably, the improvement is sufficient to mitigate the adverse effects due to the turbulence wakes from upstream turbines. The findings demonstrate that by employing a staggered design (1 device upstream and 2 devices downstream), the wake can recover its initial velocity faster due to a shorter wake generation distance.

Keywords: Grid sensitivity study, marine renewable energy, wake turbulence, vertical axis tidal turbine

1. Introduction

Globally, the amount of power produced each year is steadily increasing. The annual growth rate between 1980 and 2010 was 407 billion kWh [1]. Significant research and development of renewable energy generating technologies have occurred in recent decades to fulfil the increased electricity demand [1] caused by population growth, economic growth, industrial development, technical advancements, and rising social living standards [2]. Malaysia is also struggling to maintain consistent growth since production and maintenance expenses are rising and the country will be out of hydrocarbon resources in the next few decades [3]. Because burning fossil fuels has such negative environmental

*Corresponding author: anasrahman@unimap.edu.my

repercussions, the Malaysian government has been researching and advocating the use of renewable energy [4]. Substituting fossil fuels with renewable energy sources will lead to reliable, as well as low-cost electricity that will possess no harm to the environment [5].

Notably, Malaysia has the lowest population density among the ASEAN countries and has been actively supporting the transition towards renewable energy. Out of 13 gigawatts of total power capacity, 84% of which is produced by thermal power facilities and 16% by hydropower plants [6]. For this reason, the Malaysian government has begun looking into renewable energy sources to incorporate 20% of this type of energy into the country's overall energy mix by 2025 [7]. This is consistent with Malaysia's attempts to achieve the Sustainable Development Goals (SDGs), which are geared towards Goal 7 relating to demands for clean, affordable energy.

Tidal energy is a type of renewable energy source that is generated by the moon's and sun's gravitational forces, which cause the tide to rise and fall. It is more predictable than other renewable energy sources since it may produce energy twice a day throughout the year. Also, depending on location, it can provide a generous amount of electricity.

Tides can be categorized as diurnal, semidiurnal, and mixed tides. However, only semidiurnal and mixed tides are accessible in Malaysia, with semidiurnal being the dominant type. Spring tides have the highest currents, while neap tides have the lowest currents because the semidiurnal tide is influential in the mixed tides. As demonstrated in Fig. 1 [8], the network of tidal stations in Malaysia consists of 21 stations; 12 of which are scattered over the peninsula while the rest is located in Sarawak and Sabah.

Fig. 1 - Location of tidal stations in Malaysia [8]

Several different technologies are available in the field of tidal energy to harness the power of moving water, such as the tidal lagoon, tidal barrage, and tidal turbine [9]. The kinetic energy of the tide can be captured using either a horizontal axis tidal turbine (HATT) or a vertical axis tidal turbine (VATT). The majority of VATT research shows that this device can work in deep water, but its performance upon deployment in shallow water conditions has not been extensively investigated.

To the best of our knowledge, the Malaysian government did not issue substantial incentives for renewable energy exploration before 2021. Thus, this research was conducted using computational fluid dynamic analysis to acquire data and subsequently, perform analysis on the wake interaction caused by the deployment of vertical axis tidal turbines in shallow water for single setup and multi-rotating setup.

2. Methodology

2.1 Modelling

Darrieus turbine is a vertically oriented tidal device, with two airfoil-shaped blades that provide support (Fig. 2). The rotor is rotated by an aerodynamic force generated by the blade moving in the opposite direction of the wind. The shape of the symmetrical and non-symmetrical airfoil on the blade has a significant impact on the performance of the H-Darrieus turbine. Some of the aerodynamic series that can be used to build the blade of an H-Darrieus turbine include NACA00XX and NACA63XXX as summarized in table 1. NACA0018 airfoil design is used in this work for the H-Darrieus turbine since it has a C_p value of 0.3 (the optimal value as shown in Table 1) [10] and the blade can be constructed easily and quickly. This design is also commonly utilised in wind turbine applications for H-Darrieus turbines. Because the H-Darrieus is a lift-based turbine, increasing the thickness of the airfoil increases both the lift force and the drag force [11].

Table 1 - Power Coefficient corresponding to NACA 4-digit airfoil [12]

Symmetrical	C_p	Non-symmetrical	C_p
NACA 0010	0.2345	NACA 63418	0.2772
NACA 0015	0.2947	NACA 63415	0.1771
NACA 0018	0.2964	NACA 63412	0.1290

SOLIDWORKS software and ANSYS Fluent were used to design the geometry and analyse the simulation, respectively. As illustrated in Fig. 3, this study was carried out using different turbine setups, namely configuration A (single setup), configuration B (inline setup), and configurations C and D (staggered setup with different layouts).

Table 2 summarises the turbine, domain and also the specific spacing employed for each turbine arrangement used in this study. Lateral spacing (LS) for both configurations is 1.5D while longitudinal spacing (LGS) that is only implemented for staggered configuration is 4D. The 'D' illustrated in Fig. 3 represents the diameter of the spacing which equals 5000mm for 1D.

Table 2 -Turbine, domain and spacing parameters employed in this study

H-Darrieus Turbine Parameters		
Parameters	**Value**	
Number of blades	3	
Type of blade	NACA0018	
Chord length	1000mm	
Height	5000mm	
Diameter	4385.75mm	
Struts length	2345.99mm	
Height and diameter ratio	1	
Domain specification		
Depth	30m	
Width	80m	
Length	800m	
Turbine positioning	62.5m	
Parameter	**Lateral spacing (m)**	**Longitudinal spacing (m)**
Inline	1.5D	-
Staggered		4D

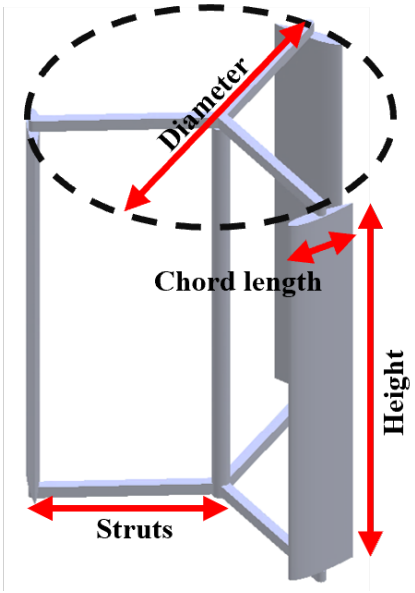

Fig. 2 - CAD drawing of H-Darrieus turbine

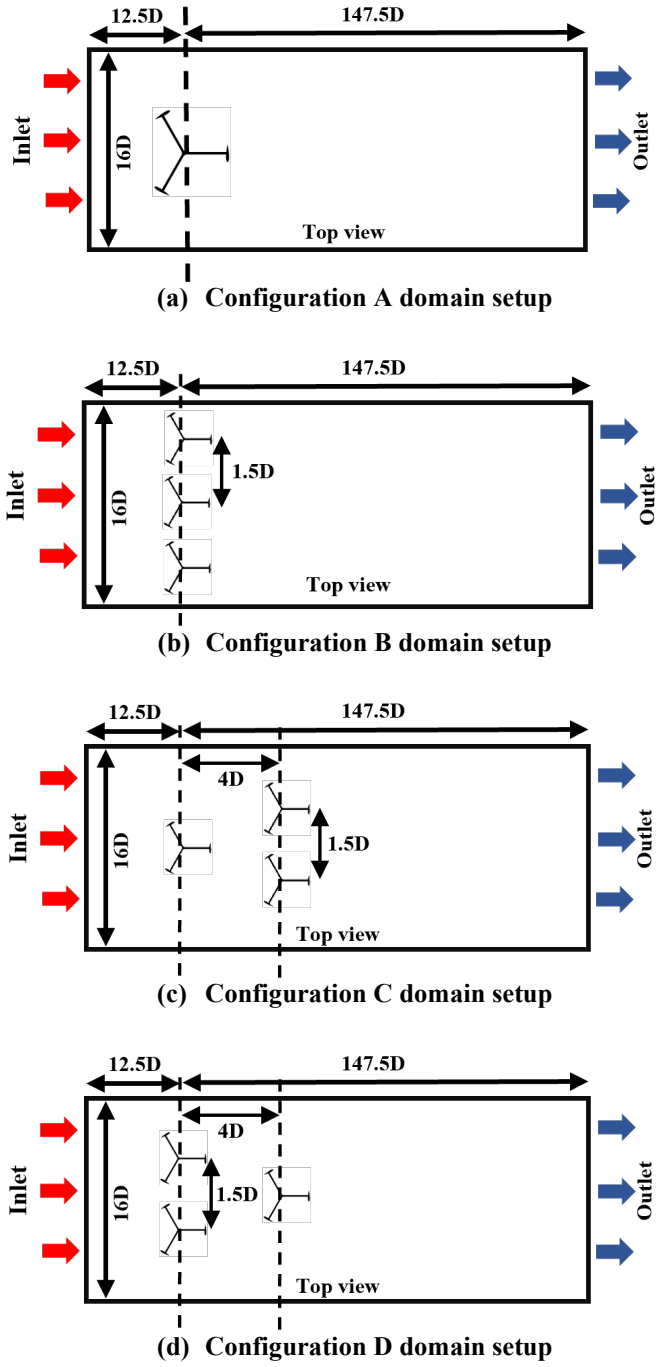

Fig. 3 - Device configuration used in this study

Suhri et al. [13] defined the study's boundary conditions as shown in Table 3 whereby the specification was employed in determining the domain of the study. The density of seawater and dynamic viscosity of water would be determined where the mean water temperature was set at 27°C. Sea water has a density of 1023 kg/m^3 and a dynamic viscosity of 0.00092 Ns/m^2. The current velocity would be 1.0 m/s.

Table 3 - Boundary condition specification

Parameter	Specification
Inlet velocity	1 m/s
Intensity turbulent	5%
Hydraulic diameter	0.1m
Viscous model	Standard k-epsilon

2.2 Mesh Independence Study

Meshing is a technique in the engineering simulation process that simplifies complex structures so that they can be used as distinct local approximations of the wider domain. The mesh has an impact on the simulations' precision, convergence, and rate. Thus, the faster and more accurate the solution is, the better and more automated the meshing procedures are.

Table 4 shows the unstructured tetra-mesh nodes and elements produced for each numerical model using Ansys Fluent with five different domain element sizes. Furthermore, mesh refinement was applied to the turbine's faces. The transition ratio is set at 0.3, the same as the face sizing with a maximum of five layers inflation was used to build up the mesh inflating technique for all types of refinement.

Table 4 also shows the number of nodes and elements in numerical simulation significantly increased when the element size of the domain and faces of the turbine are changed from very coarse to very fine refinement. As a result, the quality and accuracy of numerical study solutions may also improve. Fig. 4 shows the maximum velocity profile at 12D downstream at different types of refinement.

Table 4 - Details on grid sensitivity study conducted

Refinement	Element size (m)	Nodes	No. of Elements
Very fine	1.5	1,548,976	8,063,463
Fine	2.0	804,242	3,843,272
Medium	2.5	2,804,460	623,273
Coarse	3.0	2,348,120	542,410
Very coarse	3.5	2,115,726	500,892

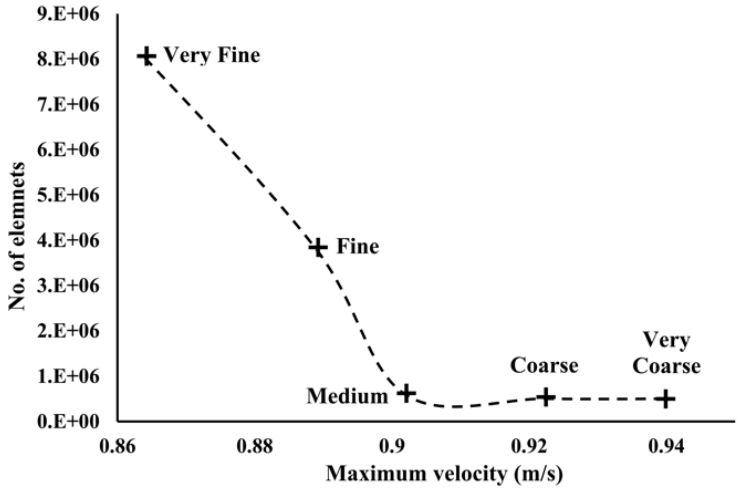

Fig. 4 - Maximum velocity at 12D downstream with different refinement levels

Nevertheless, the time it takes to generate a high-quality model influences the computation speed. It has been demonstrated that meshing with a high degree of mesh creation takes the most time. Thus, finding a numerical solution is a process of breaking the continuous geometric space of the domain and faces into smaller shapes to accurately describe the physical shape of the domain, faces, and edges. It takes the longest for a very fine model followed by medium and coarse meshing.

According to this study, changes in meshing refinement from very coarse to very fine have a considerable impact on the maximum velocity generated in numerical simulation, where slight variations in the velocity profile at different downstream locations are noticeable. As a result, fine meshing refinement was chosen as the best option for further numerical computation and analysis. Compared to mesh sizes with a finer mesh, this mesh size will give the best results and save time on calculations and analysis.

Fig. 5(a) shows the mesh of the turbine at the ZX plane while Fig. 5(b) and Fig. 5(c) show the close-up mesh of the blade and shaft of the Darrieus turbine. The skewness of the fine mesh refinement with inflation indicates a positively skewed distribution. The mode occurs near the maximum of the distribution, but the mean value surpasses the median and shifts to the right. The mean value of skewness obtained is 0.24, which is acceptable.

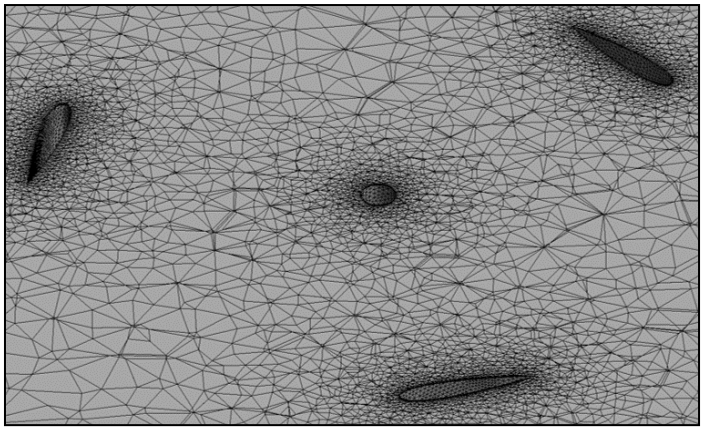

(a) Slice view highlighting the refinement of the turbine

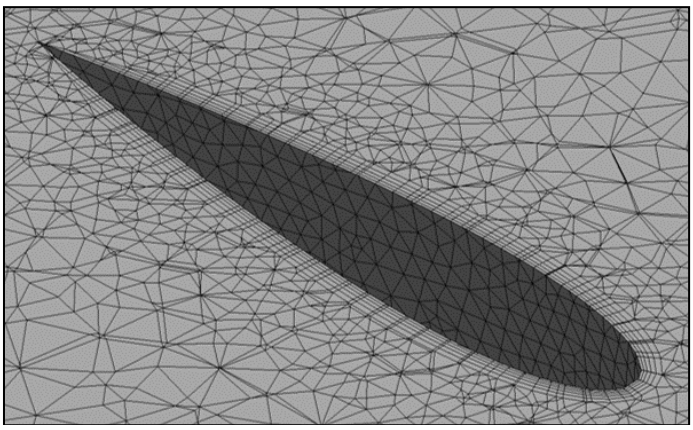

(b) Slice view highlighting the close-up fine mesh refinement of the blade

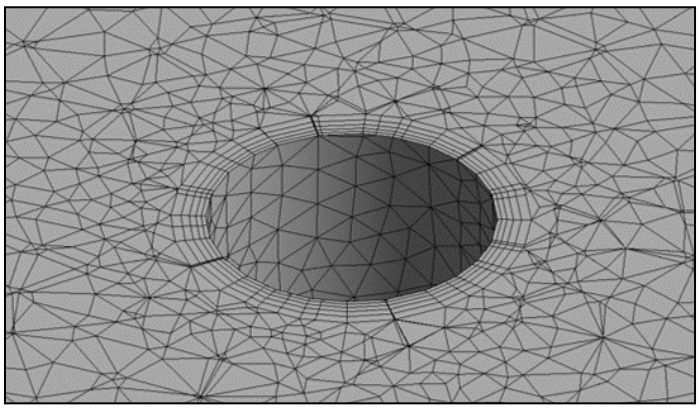

(c) Slice view highlighting the close-up fine mesh refinement of the shaft

Fig. 5 – Slices view of maximum velocity at 12d downstream with different refinement levels

2.3 Reynolds-Average Navier-Stokes Equation (RANS)

The RANS model is an equation that calculates the average flow of an incompressible fluid. When compared to Large Eddy Simulation (LES), RANS simulation will have a shorter simulation time. The steady-state RANS formulation is shown in Equation (1).

$$\rho \frac{\partial \overline{u_i}}{\partial t} + \rho \overline{u_j} \frac{\partial \overline{u_i}}{\partial x_j} = -\frac{\partial \bar{p}}{\partial x_i} + \frac{\partial}{\partial x_j}\left(\mu \frac{\overline{u_i}}{\partial x_j} - \rho \overline{u_{i'} u_{j'}}\right) \quad (1)$$

where $\bar{p}$ is time-averaged relative pressure, $-\rho\overline{u_{\iota}{}'u_{J}{}'}$ is the Reynolds stress tensor, ρ is the liquid density, and μ is the liquid's dynamic viscosity.

2.4 Standard k-epsilon Model

In any flow simulation, a standard k-epsilon model is typically used for turbulent modelling. It is a strong and reliable equation that can be applied to a wide range of engineering problems and also can produce accurate simulation results while using less computational power [14]. The transportation equation for k and ε is given below.

$$\frac{\partial}{\partial x_i}(\rho k u\bar{\imath}) = \frac{\partial}{\partial x_j}\left[\left(\mu + \frac{\mu_t}{\sigma_k}\right)\frac{\partial \varepsilon}{\partial x_j}\right] + G_k - Y_k \tag{2}$$

$$\frac{\partial}{\partial x_i}(\rho k u\bar{\imath}) = \frac{\partial}{\partial x_j}\left[\left(\mu + \frac{\mu_t}{\sigma_\varepsilon}\right)\frac{\partial \varepsilon}{\partial x_j}\right] + G_\varepsilon - Y_\varepsilon \tag{3}$$

where k is the turbulent kinetic and ε turbulent dissipation, μt is the eddy viscosity. Equations (2) and (3) show the turbulent Prandtl number which is the σk and $\sigma\varepsilon$

2.5 Tidal Stream Energy Conversion Theory

$$P = \frac{1}{2}\rho A v^3 \tag{4}$$

where ρ is the density of the fluid, A is the cross-sectional area of the turbine rotor and v is the velocity of the fluid. The cross-sectional areas (A) of HATT and VATT are distinct from one another. The cross-sectional area in the case of VATT will be:

$$A = H\ x\ D \tag{5}$$

How much energy can be extracted from a tidal current turbine can be calculated using one of several different tidal stream formulas. Using the same equation, the only distinguishing feature between tidal and wind sources would be their density. Therefore, the power output from the tidal stream current, denoted as P, is illustrated as follows [15]:

$$P = \frac{1}{2} C_p\, \rho A v^3 \tag{6}$$

where C_p is the power coefficient.

3. Result and Discussion

The simulation's output of a velocity contour is used to analyse the wake behaviour in three distinct setups. The velocity deficiency was further analysed using the normalized velocity plot. This study also will be validated with two experimental data from [16] and [17].

3.1 Comparison Between Experimental Data and Simulation Data

The first step was to compare VATT cylindrical design to the Darrieus turbine designed for this study. To study the wake turbulence caused by the two distinct geometries, the cylindrical design was recreated using the previously discussed characteristics as done by Suhri [13]. As can be seen in Fig. 6, the Darrieus turbine produces a larger wake than the hypothetical cylinder as shown in Fig. 7. Maximum velocities of 1.2 m/s are observed at the object's top and bottom for cylinder designs, whereas for the Darrieus turbine, they were measured at the NACA blade's tip.

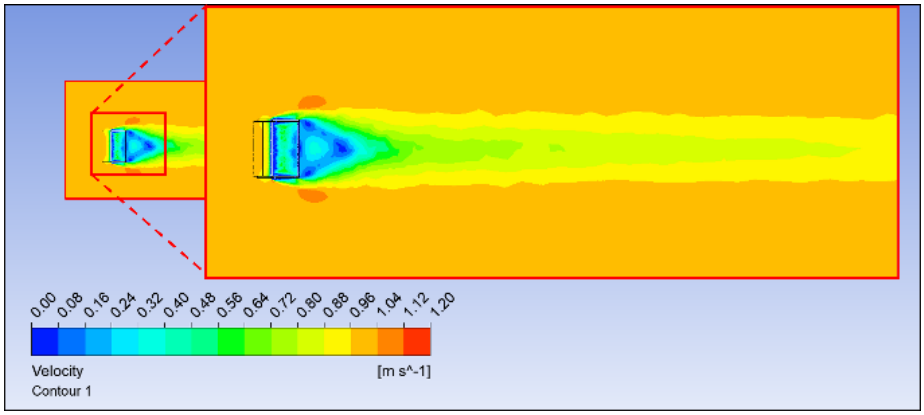

(a) side view of the domain

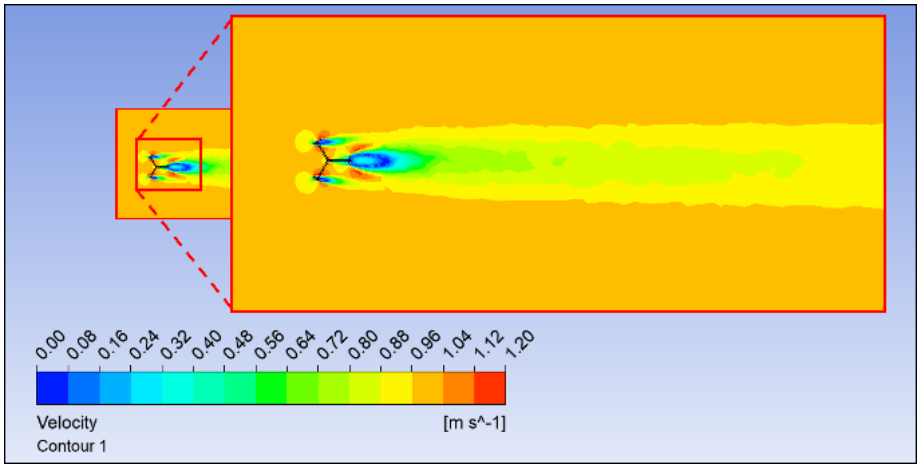

(b) top view of the domain

Fig. 6 - Velocity contour of the Darrieus turbine

The Darrieus turbine creates a more extensive and longer wake than the hypothetical cylinder, accounting for 4.1% of the percentage difference. This is because the turbine's blades affect the incoming flow as it travels through the turbine.

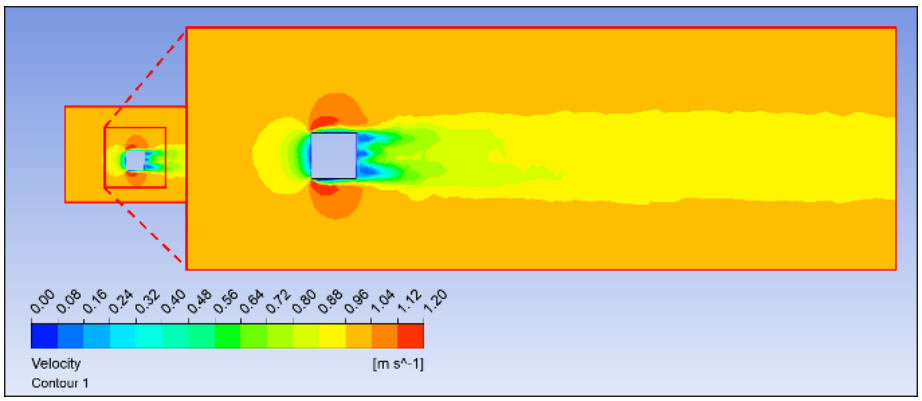

(a) side view of the domain

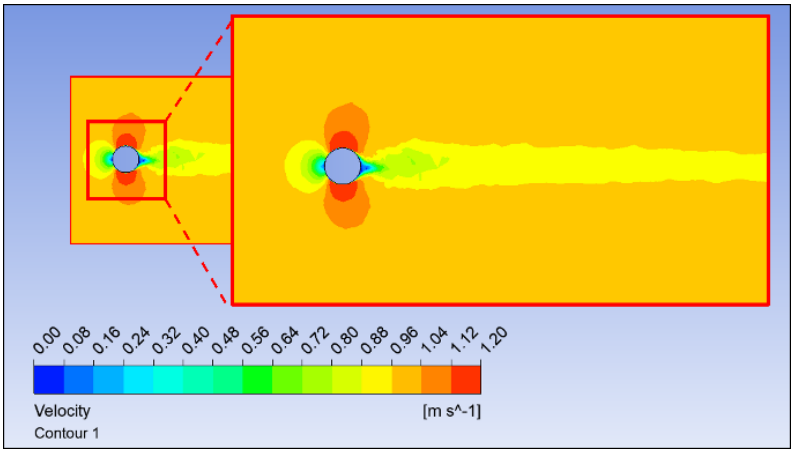

(b) top view of the domain

Fig. 7 - Velocity contour of a cylindrical object

The study then proceeds by evaluating the simulation result for configuration A, which consists of a single turbine, to an experimental result obtained by Clary et al. [16], who used the Darrieus turbine model in the study. The wake slicing point is the location where the turbulence data is extracted for analysis. For this study, three extraction points were selected at 6D, 8D, 10D, and 12D, where D refers to the downstream position from the turbine and the numbers reflect the extraction location. For example, 8D refers to the downstream distance of 40 metres, in which 8 metres x 5 metres of turbine diameter.

Fig. 8(a) shows the velocity deficit at 6D downstream, where the wake begins to rebound to the initial velocity at 0.84 m/s, which accounts for 6.47% of the percentage difference between experimental data and simulated results. The percentage is subsequently increased to 3.08%, resulting in a percentage deviation of 9.55% at 8D downstream, which begins to recover to the initial velocity at 0.86 m/s, shown in Fig. 8(b). At 12D downstream, the wake begins to recover at 0.89 m/s, as can be seen in Fig. 8(c), which is closer to the beginning velocity and has a percentage deviation reduction of 9.02%, which is shown in Table 5.

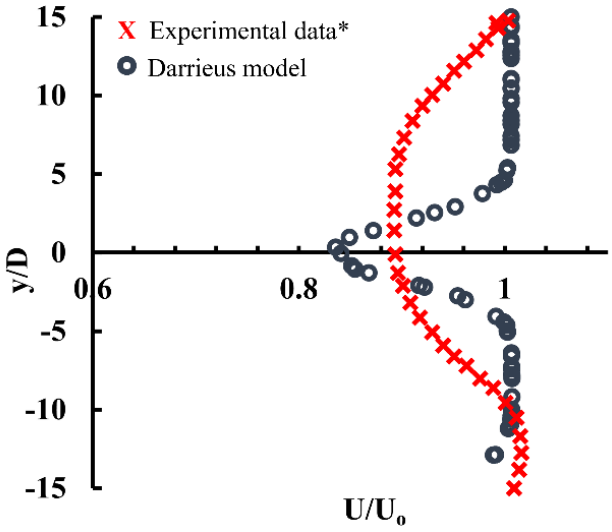

(a) Velocity magnitude at 6D downstream

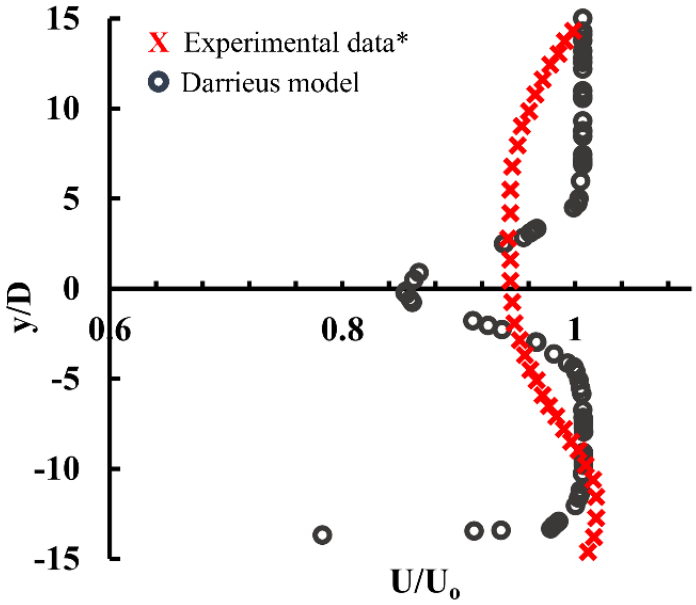

(b) Velocity magnitude at 8D downstream

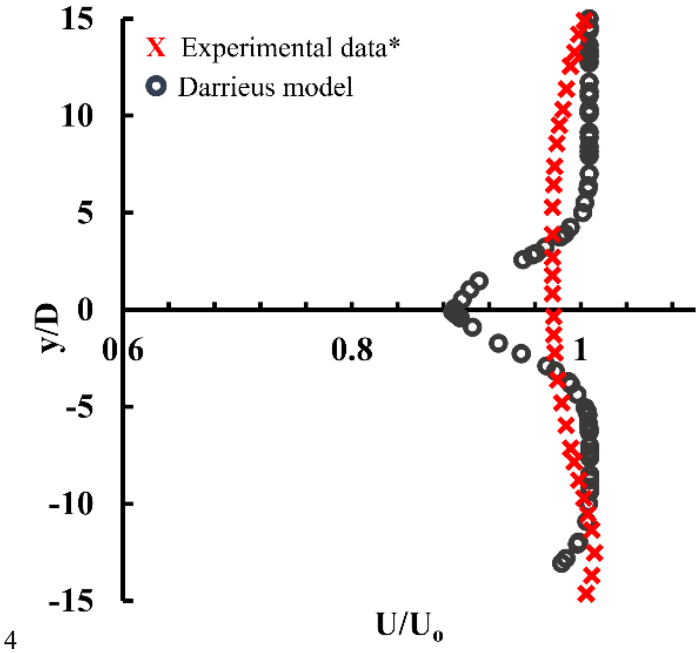

4

(c) Velocity magnitude at 12D downstream

Fig. 8 - Velocity magnitude with different downstream of configuration A

Table 5 - Percentage deviation for configuration A in three locations

Experimental data vs current study	
Darrieus turbine	**NACA0018**
% Percentage deviation (6D)	6.47%
% Percentage deviation (8D)	9.55%
% Percentage deviation (12D)	9.02%

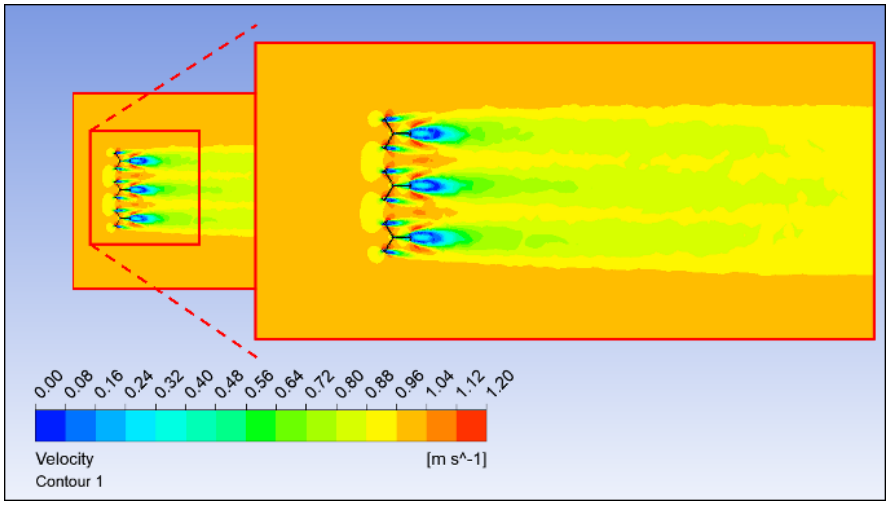

Fig. 9 - Velocity contour for configuration B

This study is focused on shallow water array installations since a single row of turbines is less efficient when applied to a wide region [6]. Like the single turbine simulation, the three-turbine simulation had been executed with a well-refined mesh. Referring to Fig. 9, configuration B is a single row of three turbines with 1.5D hub-to-hub spacing. Once the incoming flow reaches the turbines, the velocity distribution indicates that it accelerates on the row's sides and between the turbines. Additionally, it illustrates the high-velocity wakes behind each device, which does not converge until 12D downstream.

The velocity deficit at 8D downstream, where the wake begins to rebound to the initial velocity at 0.85 m/s, accounts for 8.02 of the mean absolute difference between experimental data from Stallard et al. [17] and simulation results. Fig. 10(a) shows at 8D downstream, the velocity deficit varies minimally. The velocity deficit is almost consistent across the wake width after 8D downstream. The mean absolute error is then increased to 9.3 at 10D downstream when the velocity begins to recover to 0.86 m/s as seen in Fig. 10(b) . The wake begins to recover at 0.87 m/s downstream, which is closer to the starting velocity as plotted in Fig. 10(c) and has a mean absolute error decrease of 8.8, as shown in Table 6 mean absolute error of configuration B. The plot's trend revealed that there is a disparity between the experimental and Darrieus models, which resulted due to the different simulation methods used.

Table 6 - Mean absolute error of configuration B

Downstream	**8D**	**10D**	**12D**
Mean absolute error	8.2	9.3	8.8

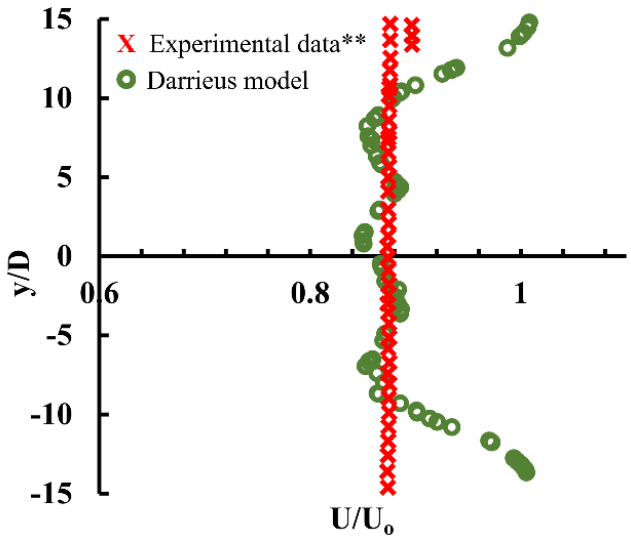

(a) Velocity magnitude at 8D downstream

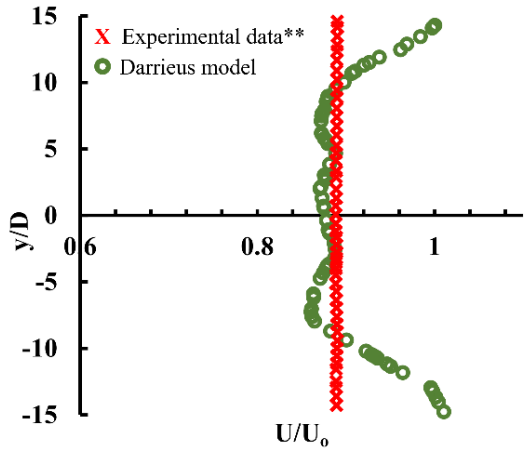

(b) Velocity magnitude at 10D downstream

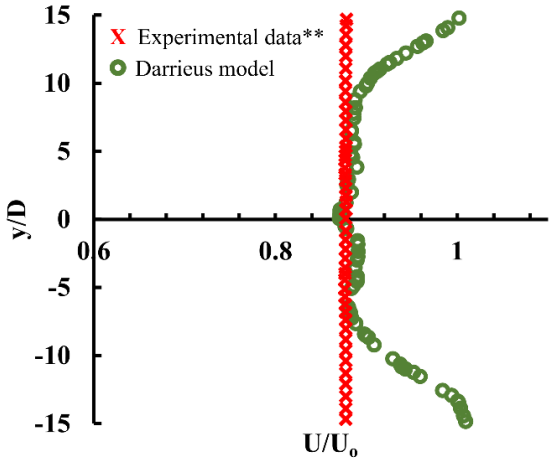

(b) Velocity magnitude at 12D downstream

Fig. 10 - Velocity magnitude with different downstream of configuration B

Next simulations were run using configurations C and D (refer to Fig. 11 and Fig. 12), where the parameters setup was the same as in Olczak et al. [18] simulation, using 1.5D for Lateral Spacing (LS) and 4D for Longitudinal Spacing (LGS). The configuration is for three turbine devices with one upstream and two downstream, while the other is for three turbine devices, two upstream and one downstream.

In compliance with the velocity distribution, once the incoming flow reaches the turbines, it accelerates on the row's sides and between the turbines. It exhibits a higher acceleration when it first contacts the turbine surface and a lower acceleration after passing through the turbine. The maximum velocity at the tip of the NACA airfoil is 1.2 m/s. The simulation also demonstrates that the wake recovers within a short distance, which is a decent performance for the turbine.

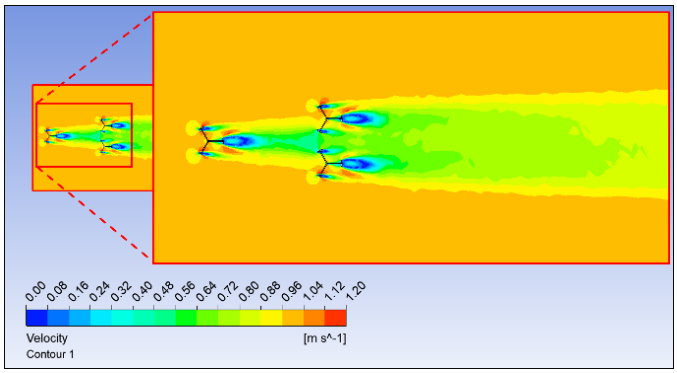

Fig. 11 - Velocity contour for configuration C

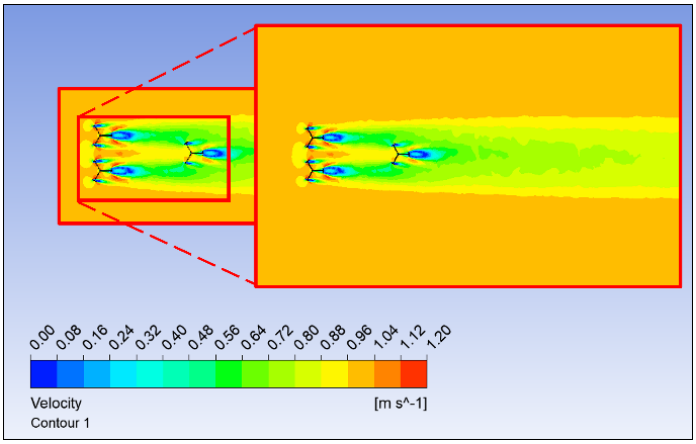

Fig. 12 - Velocity contour of configuration D

The high mixing energy from the two devices upstream influenced the downstream turbine, which runs on its own. Due to the low performance, the wake takes a longer distance to recover. The scatter plot in Fig. 13 shows the velocity magnitude of the turbine at 12D downstream. It shows that the velocity for one device upstream has begun to return to the initial velocity, with the lowest velocity of 0.79 m/s at 12D downstream, while the velocity for two devices upstream began to recover to the ambience velocity of 0.77 m/s.

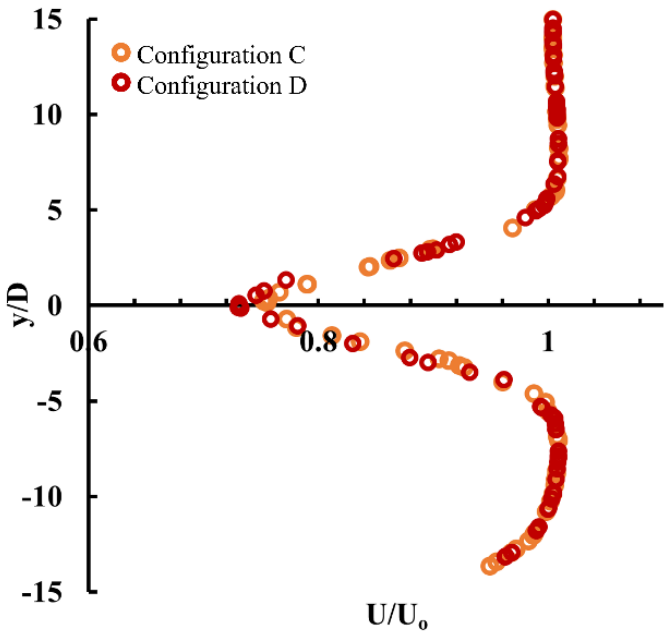

Fig. 13 - Comparison between velocity magnitude at 12D downstream between configurations C and D

The absolute error of the velocity is 2%, that shown in Table 7 proves that positioning two devices side by side at downstream, it helps to expand the configuration's effectiveness at an incoming flow velocity of 1.0 m/s. Hence, configuration C was used in the comparison against configurations A and B.

Table 7 - Absolute error for configurations C and D

Configuration	Maximum value (m/s)	Absolute error (%)
C	0.79	2%
D	0.77	

3.2 Velocity Deficit with Different Configuration

Different configurations, including configuration A, configuration B, and configuration C were then compared with their relative velocity as illustrated in Fig. 14. Data for inline and staggered setups were evaluated with single turbine data as needed to determine the best turbine positioning that will yield the best performance. Table 8(a) shows the absolute error of velocity magnitude at 8D downstream. The absolute error for inline configuration is 2.4%, while the absolute error for staggered configuration is 11.7%, representing a 9.8% increase in percentage. While the velocity of the staggered arrangement began to recover at 0.75 m/s at 8D downstream, the inline setup only began to recover at 0.84 m/s.

According to Table 8(b), the velocity of the staggered arrangement began to recover to its initial velocity at 0.77 m/s with an absolute error of 9.7% at a distance of 10D downstream. There was a 9.1% reduction in absolute error as the inline configuration started to recover at 0.86 m/s with a 0.6% of absolute error. The staggered configuration begins to recover at a velocity of 0.79 m/s at a distance of 12D downstream with an absolute error percentage of 9.2%, as shown in Table 8(c). In the inline setup, the velocity starts to recover at 0.87 m/s with a percentage rate of 0.8% absolute error. It represents about 8.4% drop in proportion.

Table 8 - Absolute error of array velocity deficit at three different downstream

(a) Velocity deficit at 8D downstream

Configuration		Single turbine	Absolute error
Inline	0.842714	0.866991	2.4
Staggered	0.750164		11.7

(b) Velocity deficit at 10D downstream

Configuration		Single turbine	Absolute error
Inline	0.860582	0.86662	0.6
Staggered	0.769518		9.7

(c) Velocity deficit at 12D downstream

Configuration		Single turbine	Absolute error
Inline	0.870369	0.878045	0.8
Staggered	0.785597		9.2

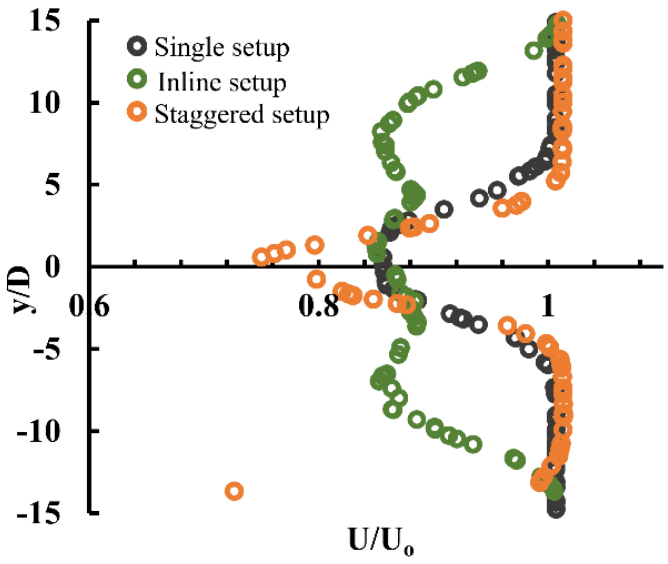

(a) Velocity magnitude at 8D downstream

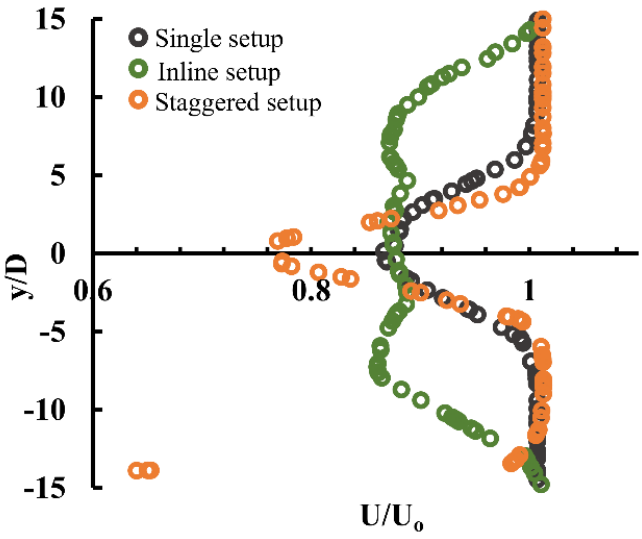

(b) Velocity magnitude at 10D downstream

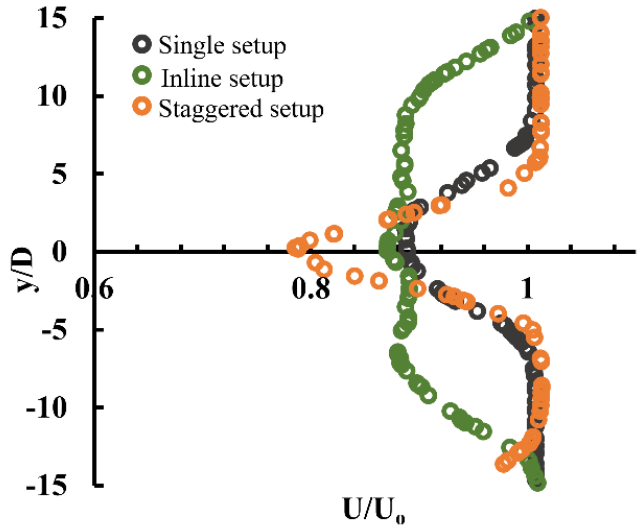

(c) Velocity magnitude at 12D downstream

Fig. 14 - Velocity magnitude at different downstream for distinct turbine setup arrangement

4. Conclusion

This study aims to analyse wake characteristics for a single setup and multi-row configuration of the Darrieus tidal turbine for shallow water applications. To satisfy energy production requirements, the turbine array was arranged into different rows that include the turbine's upstream and downstream. The turbine was deployed in staggered designs to reduce the bad influence of wake. A staggered configuration with 1 device upstream and 2 devices downstream surpassed another setup with 2 devices upstream and 1 device behind with 2% of the absolute error. At each specified distance, the wake of the velocity recovery with 1 upstream device recovered faster towards its initial velocity.

The analysis also showed that there was no difference in recovery time between a single turbine and inline configurations because there was no turbine downstream. The wake recovery of a staggered setup was slower as the flow from upstream needs to pass through the interaction of the downstream turbine.

To conclude, numerical models that were developed in this study demonstrate appropriate behaviour expected for the three-turbine array configuration, indicating that two turbines side by side installation could produce a massive performance improvement. This setup started to recover at 0.76 m/s, which was 0.3 m/s faster than the configuration with a single device downstream. Significantly, this performance boost is needed to cover for the adverse effects due to wakes from the upstream turbines.

Acknowledgement

The authors gratefully acknowledge the support received from the Ministry of Higher Education Malaysia through the Fundamental Research Grant Scheme for Research Acculturation of Early Career Researchers (FRGSRACER) RACER / 1 / 2019 / TK07 / UNIMAP/1. Additionally, the authors are also thankful for the support received from Universiti Malaysia Perlis, specifically from the Research Management Centre (RMC).

References

[1] B. Daniel and J. Nicklas, "The Development of a Vertical Axis Tidal Current Turbine," *KTH Ind. Eng. Manag.*, p. 84, 2013, [Online]. Available: http://www.diva-portal.org/smash/record.jsf?pid=diva2:537660&dswid=6120.

[2] D. Satrio and I. Ketut Aria Pria Utama, "Proceeding of Ocean, Mechanical and Aerospace-Science and Engineering Vertical Axis Tidal Current Turbine: Advantages and Challenges Review," vol. 3, no. November, 2016.

[3] N. Gomesh, I. Daut, M. Irwanto, Y. M. Irwan, and M. Fitra, "Study on Malaysian's perspective towards renewable energy mainly on solar energy," *Energy Procedia*, vol. 36, pp. 303–312, 2013, doi: 10.1016/j.egypro.2013.07.035.

[4] M. N. Chik, "Simulation Studies on the Electrical Power Potential Harnessed by Tidal Current Turbines," *J. Energy Environ.*, pp. 1–12, 2017.

[5] E. Septyaningrum *et al.*, "Performance analysis of multi-row vertical axis hydrokinetic turbine-straight blade cascaded (VAHT-SBC) turbines array," *J. Mech. Eng. Sci.*, vol. 13, no. 3, pp. 5665–5688, 2019, doi: 10.15282/jmes.13.3.2019.28.0454.

[6] B. Bakhtyar, K. Sopian, M. Y. Sulaiman, and S. A. Ahmad, "Renewable energy in five South East Asian countries: Review on electricity consumption and economic growth," *Renew. Sustain. Energy Rev.*, vol. 26, no. October, pp. 506–514, 2013, doi: 10.1016/j.rser.2013.05.058.

[7] W. S. W. Abdullah, M. Osman, M. Z. A. A. Kadir, and R. Verayiah, "The potential and status of renewable energy development in Malaysia," *Energies*, vol. 12, no. 12, 2019, doi: 10.3390/en12122437.

[8] L. W. Koon, "Investigation of Tidal Power Potentials in," *Water Resour. Environ. Syst. Div.*, vol. 5, no. 3, p. 922, 2006.

[9] N. A. Mohd Yusoff, N. L. Ramli, and M. R. Mohamed, "Investigation of the potential harnessing tidal energy in Malaysia," *ARPN J. Eng. Appl. Sci.*, vol. 10, no. 21, pp. 9835–9841, 2015.

[10] M. J. T. Loutun *et al.*, "2d cfd simulation study on the performance of various naca airfoils," *CFD Lett.*, vol. 13, no. 4, pp. 38–50, Apr. 2021, doi: 10.37934/cfdl.13.4.3850.

[11] M. J. Alam and M. T. Iqbal, "A low cut-in speed marine current turbine," no. December, pp. 1–9, 2020.

[12] M. H. Mohamed, "Performance investigation of H-rotor Darrieus turbine with new airfoil shapes," *Energy*, vol. 47, no. 1, pp. 522–530, 2012, doi: 10.1016/j.energy.2012.08.044.

[13] G. Suhri, A. Abdul Rahman, L. Dass, and K. Rajendran, "Interaction Between Tidal Turbine Wakes: Numerical Study of Shallow Water Application," vol. 1, pp. 1–5, 2020.

[14] N. Mulvany, L. Chen, J. Tu, and B. Anderson, "Steady-State Evaluation of Two-Equation RANS (Reynolds-Averaged Navier-Stokes) Turbulence Models for High-Reynolds Number Hydrodynamic Flow Simulations," *Dep. Defence, Aust. Gov.*, pp. 1–54, 2004, [Online]. Available: http://oai.dtic.mil/oai/oai?verb=getRecord&metadataPrefix=html&identifier=ADA426359.

[15] D. Satrio and I. Ketut Aria Pria Utama, "Vertical Axis Tidal Current Turbine: Advantages and Challenges Review," *Proceeding Ocean. Mech. Aerosp.*, vol. 3, no. July 2020, pp. 64–71, 2016.

[16] V. Clary, T. Oudart, P. Larroudé, J. Sommeria, and T. Maître, "An optimally-controlled RANS Actuator force model for efficient computations of tidal turbine arrays," *Ocean Eng.*, vol. 212, no. October 2019, 2020, doi: 10.1016/j.oceaneng.2020.107677.

[17] T. Stallard, R. Collings, T. Feng, and J. Whelan, "Interactions between tidal turbine wakes: Experimental study of a group of three-bladed rotors," *Philos. Trans. R. Soc. A Math. Phys. Eng. Sci.*, vol. 371, no. 1985, 2013, doi: 10.1098/rsta.2012.0159.

[18] A. Olczak, T. Stallard, T. Feng, and P. K. Stansby, "Comparison of a RANS blade element model for tidal turbine arrays with laboratory scale measurements of wake velocity and rotor thrust," *J. Fluids Struct.*, vol. 64, pp. 87–106, 2016, doi: 10.1016/j.jfluidstructs.2016.04.001.